Geophys. J. R. astr. Soc. (1985) **80**, 677–693

The evolution of the Gulf of Corinth (Greece): an aftershock study of the 1981 earthquakes

G. C. P. King *Bullard Laboratories, Madingley Rise, Madingley Road, Cambridge CB3 0EZ*

Z. X. Ouyang *Seismo-geological expedition, State Seismological Bureau, Beijing, China*

P. Papadimitriou, A. Deschamps and J. Gagnepain *Instutut de Physique du Globe, LEGSP, Universite Pierre et Marie Curie, 4 Place Jussieu, 75230 Paris Cedex 05, France*

G. Houseman *Earth Sciences, ANU, GPO Box 4, Canberra, ACT 2601, Australia*

J. A. Jackson *Bullard Laboratories, Madingley Rise, Madingley Road, Cambridge CB3 0EZ*

C. Soufleris *Western Geophysical, PO Box 2469, Houston, Texas 7725, USA*

J. Virieux *Institut de Physique du Globe, LEGSP, Universite Pierre et Marie Curie, 4 Place Jussieu, 75230 Paris Cedex 05, France*

Accepted 1984 August 13. Received 1984 August 13; in original form 1984 March 8

Summary. A preliminary study of the aftershocks of three earthquakes that occurred near to Corinth (Greece) in 1981 is combined with observations of the morphology and faulting to understand the evolution of the Eastern Gulf of Corinth. The well located aftershocks form a zone 60 km long and 20 km wide. They do not lie on the main fault planes and are mostly located between the north-dipping faulting on which the first two earthquakes occurred and the south-dipping faulting associated with the third event. A cluster of aftershocks also lies in the footwall of the eastern end of the south-dipping fault of the third event.

Morphologically, it is observed that in the evolution of the Eastern Gulf of Corinth, antithetic faulting apparently predates the appearance of the main faulting at the surface. This evolution can be explained by motion on a deep seated, shallow angle, aseismic normal fault. A model based on such a fault also accounts for the aftershock distribution of the 1981 earthquakes.

1 Introduction

On 1981 February 24, 25 and March 4, three earthquakes of magnitudes M_S 6.7, 6.4 and 6.4 (USGS) occurred in the eastern part of the Gulf of Corinth (Fig. 1). Surface breaks, with a

northward-dipping slip vector, were noticed on the southern side of the Gulf following the first and second events and further fresh faulting with a southward dip appeared later on the northern side of the Gulf as a result of the March 4 event.

By March 4 a network of MEQ-800 portable smoked-drum seismographs belonging to the Universities of Cambridge and Thessaloniki and operated by people from Cambridge, Thessaloniki and Paris was set-up in the area. The array remained operational for five weeks and at the same time studies of surface faulting, shoreline changes and morphology were carried out. A description of this work together with relocations and waveform studies of the main events using teleseismic *P*-waves are discussed in an earlier paper by Jackson *et al.* (1982) (subsequently we refer to this paper as [1]). The work on changes of shorelines and faulting has since been extended and forms a separate study (Vita-Finzi & King 1984). Here we are mainly concerned with a discussion of the first results of the aftershock study. The results are preliminary in that we examine only 133 of the larger events whereas work in progress will locate rather more than 10 times this number. From among the events, 70 are very well located and 26 of these provide reliable fault plane solutions. The data support a view suggested by the morphology and fault mapping that, in the evolution of the Gulf of Corinth and possibly other rift systems, antithetic faulting can precede the surface appearance of the main faulting. A plausible mechanism for this is described.

Earthquake location accuracy is difficult to quantify reliably. The most convenient estimates determine the stability of the locations and ignore other sources of error. For this reason careful tests have been carried out to ensure that our locations are reliable. These tests are described in the next section but will only be published in full when an analysis of all the data is complete.

2 Data reduction

The data were read using a high resolution digitizing table. In previous work (Berberian 1982; Soufleris *et al.* 1982; Yielding *et al.* 1981; Deschamps & King 1984) it has been argued that the reading error of smoked drum records using this technique is 0.15 s for *P*-waves and 0.3 s for *S*-waves. The earthquakes were located using the HYP071 location program (Lee & Lahr 1975) assigning *S*-wave arrivals one-fourth of the weight of *P*-wave arrivals. Because of the way in which weight is defined in the version of HYP071 used in Cambridge, this means that an *S*-wave residual is actually assigned half of the importance of a *P*-wave residual. Since *S*-waves travel at about half the speed of *P*-waves the net effect is that the *S*-wave readings control epicentral position as firmly as *P*-wave readings. Since combined *S*- and *P*-wave readings together reduce the trade-off between the location and origin time the net effect of using *S*-waves is to produce more reliable locations. This is despite the fact that *S*-wave arrivals on vertical component seismometers may be confused with arrivals due to *P*-wave to *S*-wave conversion giving occasional errors of 0.5 s and despite the fact that rms residuals using *P*-waves alone are substantially lower. The better rms using *P*-wave readings alone arises from a trade-off between the origin time and location and does not indicate a better location.

The positions of the stations used for the locations are shown in Fig. 1 and were at a range of heights (Table 1). Each station was therefore assigned a time correction according to its altitude relative to the lowest station. These were based on a choice of mean near surface velocity of 4.5 km s^{-1}. The largest correction (0.11 s) is less than the reading error and any of the rms residuals of the location procedure, so the choice of a velocity of 4.5 km s^{-1} for the surface layer is not important.

The velocity of the crust 50 km south of the region is available from a refraction study (Makris 1977) which gives a 15 km layer with a velocity of 6.0 km s^{-1} overlying a layer

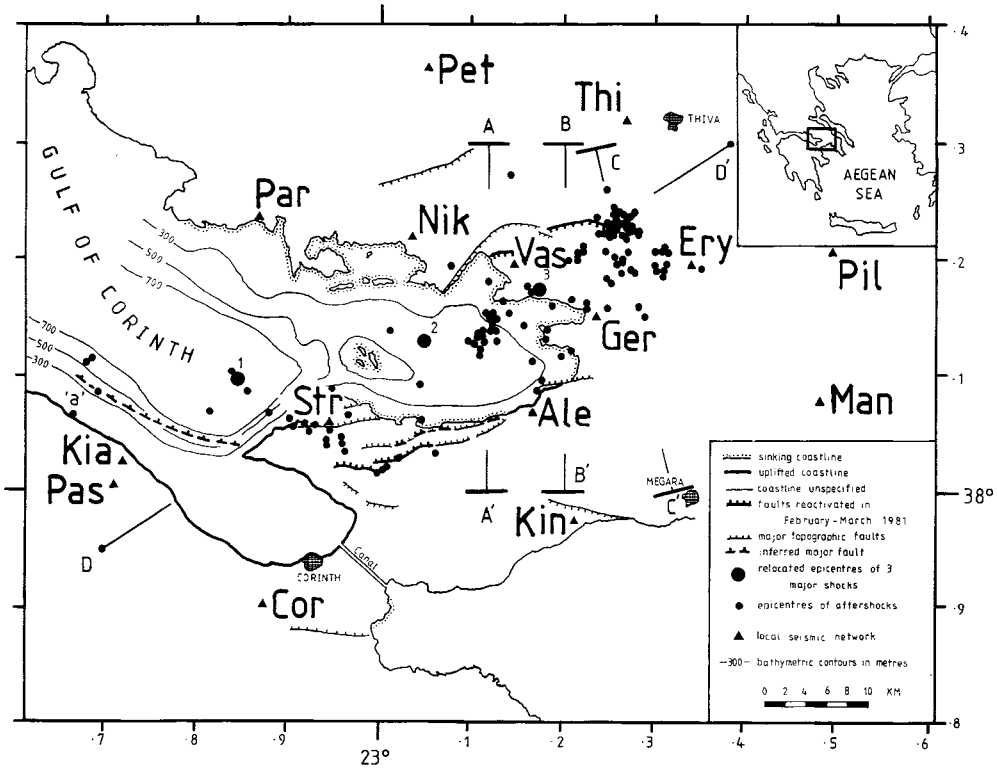

Figure 1. Location and summary map (for place names see Fig. 6). Epicentres of the February 24 (1), 25 (2) and March 4 (3) earthquakes are from [1]. The lines of the sections in Figs 2 and 3 are shown. Bars indicate the width of the projection zone for AA′, BB′ and CC′. The aftershock 'a' is discussed in the text.

Table 1

	STATION	LATITUDE (Degrees, Minutes)	LONGITUDE (Degrees Minutes)	HEIGHT (metres)	TIME CORRECTION (seconds)	PERIOD OF OPERATION (1981)
1	KIN	37 58.98N	23 13.80E	50	+0.01	5 MARCH-30 MARCH
2	STR	38 03.54N	22 56.76E	50	+0.01	8 MARCH-30 MARCH
3	PET	38 23.28N	23 00.48E	100	+0.02	6 MARCH-31 MARCH
4	ERY	38 11.88N	23 20.52E	500	+0.11	6 MARCH-31 MARCH
5	VAS	38 11.76N	23 08.82E	150	+0.03	9 MARCH-31 MARCH
6	KIA	38 01.50N	22 43.24E	50	+0.01	5 MARCH-18 MARCH
7	PIL	38 12.54N	23 29.64E	500	+0.11	15 MARCH-30 MARCH
8	MAN	38 05.16N	23 28.74E	150	+0.03	6 MARCH-30 MARCH
9	COR	37 53.82N	22 52.38E	100	+0.02	5 MARCH-30 MARCH
10	PAS	38 00.30N	22 42.66E	100	+0.02	19 MARCH-30 MARCH
11	THI	38 19.20N	23 16.38E	300	+0.07	6 MARCH-27 MARCH
12	GER	38 08.94N	23 14.94E	50	+0.01	6 MARCH-31 MARCH
13	PAR	38 14.04N	22 52.08E	0	0.00	8 MARCH-30 MARCH
14	ALE	38 04.02N	23 08.94E	50	+0.01	9 MARCH-30 MARCH
15	NIK	38 13.14N	23 02.16E	100	+0.02	8 MARCH-31 MARCH

with a velocity of 7.2 km s^{-1}. For initial tests we therefore chose a 6.0 km s^{-1} half-space and examined seven events with more than five *P*-wave and five *S*-wave arrival readings. The locations using this model were used to construct a Wadati plot (*P*-wave travel time plotted against *S*-wave minus *P*-wave travel time). A mean v_p/v_s ratio of 1.83 was found by this method and adopted for the further tests.

A larger group of 70 events (indicated by asterisks in Table 2), all of which had more than five *P*-wave arrivals and two *S*-wave arrivals were then located in half-spaces of constant

Table 2

	Date (year, month, day)	Origin Time (hour, minute, second)	Latitude	Longitude	Depth (km)	RMS (seconds)	ERH (km)	ERZ (km)	No. of Readings Q	P	S
*	810307	0 3 50.40	38 12.40 N	23 18.77 E	5.67	0.12	0.60	1.00	B	8	2
*	810307	0 39 17.44	38 11.74 N	23 17.98 E	7.13	0.11	0.60	0.60	B	8	2
	810307	1 48 38.93	38 11.58 N	23 21.03 E	1.25	0.09	0.50	0.90	B	7	2
	810307	6 0 13.67	38 11.79 N	23 18.79 E	0.13	0.06	0.30	10.30	C	6	3
	810307	13 34 43.04	38 9.50 N	23 14.92 E	10.60	0.09	0.80	1.40	B	7	0
	810307	16 36 50.03	38 13.48 N	23 16.33 E	6.84	0.11	0.50	0.80	B	8	4
	810307	17 49 12.30	38 13.31 N	23 15.14 E	7.27	0.11	0.50	0.70	B	8	4
	810307	18 27 36.07	38 3.92 N	22 58.00 E	5.00	0.13	0.60	1.10	B	10	3
	810307	18 52 12.19	38 3.12 N	22 55.45 E	0.35	0.17	0.70	5.50	C	8	3
*	810307	18 54 33.92	38 12.44 N	23 18.49 E	3.61	0.10	0.50	1.00	B	9	2
1*	810307	19 39 40.36	38 9.56 N	23 16.96 E	11.37	0.06	0.30	0.40	A	8	3
	810307	21 19 12.29	38 12.60 N	23 18.66 E	2.71	0.09	0.50	1.00	B	9	1
2*	810307	22 12 58.66	38 10.83 N	23 15.11 E	7.30	0.09	0.50	0.90	A	8	2
•	810307	23 21 39.90	38 11.33 N	23 15.79 E	6.55	0.07	0.30	0.40	A	9	3
•	810308	0 49 42.56	38 12.14 N	23 15.37 E	8.64	0.08	0.30	0.40	A	9	4
	810308	2 14 36.98	38 2.81 N	22 57.55 E	1.55	0.11	0.50	1.30	B	9	2
*	810308	4 18 19.12	38 9.04 N	23 7.20 E	8.18	0.08	0.40	1.30	B	9	2
*	810308	4 31 21.82	38 9.19 N	23 7.05 E	8.10	0.07	0.20	0.60	B	10	4
	810308	6 41 23.48	38 11.35 N	23 16.65 E	1.86	0.10	0.40	1.50	B	8	2
	810308	9 23 59.51	38 12.02 N	23 15.90 E	8.47	0.07	0.50	0.70	A	7	2
*	810308	12 12 41.41	38 4.13 N	22 48.95 E	12.59	0.12	0.70	0.80	B	10	2
	810308	13 25 0.36	38 3.19 N	22 56.80 E	0.26	0.12	0.40	1.30	B	7	1
	810308	14 17 36.31	38 13.97 N	23 14.83 E	4.90	0.08	0.40	1.00	B	9	2
	810308	17 26 36.39	38 11.18 N	23 18.53 E	5.00	0.09	0.70	1.00	B	7	2
3*	810308	18 25 36.12	38 9.95 N	23 12.54 E	6.36	0.06	0.30	0.50	A	9	3
*	810309	4 21 27.91	38 12.42 N	23 14.78 E	7.59	0.10	0.40	0.70	A	10	3
	810309	7 4 13.02	38 1.77 N	23 1.26 E	1.91	0.11	0.70	3.80	C	10	0
	810309	13 18 49.87	38 1.26 N	23 0.48 E	3.43	0.11	0.80	2.00	B	9	1
*	810309	15 7 39.56	38 11.42 N	23 18.09 E	4.12	0.09	0.40	0.50	B	9	4
	810309	15 32 19.80	38 11.40 N	23 16.56 E	1.01	0.09	0.40	3.00	B	7	2
	810309	19 53 31.43	38 8.36 N	23 7.36 E	5.92	0.11	0.50	0.80	B	10	3
*	810309	21 22 17.83	38 10.64 N	23 9.67 E	7.21	0.14	0.60	0.60	A	10	3
	810309	22 25 42.28	38 16.39 N	23 8.55 E	9.99	0.11	0.90	1.50	C	10	1
	810309	23 52 13.59	38 8.11 N	23 6.45 E	6.30	0.12	0.60	1.70	B	10	1
	810310	1 7 16.03	38 8.31 N	23 0.75 E	8.92	0.12	1.20	2.60	C	8	0
	810310	4 25 15.87	38 11.95 N	23 15.88 E	3.36	0.07	0.40	1.00	B	10	1
	810310	5 6 15.52	38 1.99 N	23 3.71 E	3.89	0.09	0.60	2.20	B	9	0
	810310	8 32 52.27	38 7.77 N	23 6.84 E	8.69	0.07	0.40	0.90	B	10	0
	810310	10 19 16.83	38 2.54 N	22 56.59 E	1.86	0.02	0.20	0.30	B	6	0
*	810310	16 30 50.66	38 12.63 N	23 13.38 E	8.80	0.04	0.30	0.30	B	8	2
	810310	16 46 47.11	38 7.34 N	23 6.64 E	7.31	0.08	0.50	0.80	B	10	1
4*	810310	19 7 34.02	38 11.73 N	23 15.46 E	4.86	0.11	0.50	0.80	B	10	2
	810311	8 48 13.56	38 2.06 N	22 57.78 E	0.28	0.18	0.60	9.90	C	8	0
	810311	9 34 11.10	38 13.27 N	23 15.85 E	3.17	0.08	0.50	1.90	B	10	0
	810311	11 18 44.61	38 2.51 N	22 57.60 E	0.55	0.17	0.70	5.20	C	11	2
	810311	13 11 48.41	38 13.10 N	23 16.09 E	4.69	0.07	0.30	0.60	B	10	3
*	810311	13 56 40.70	38 11.98 N	23 12.94 E	5.22	0.11	0.40	0.60	B	11	2
	810311	15 36 40.60	38 2.65 N	23 56.60 E	2.35	0.10	0.70	1.20	B	8	0
	810311	18 16 23.98	38 13.40 N	23 16.93 E	3.66	0.07	0.40	1.00	B	10	1
	810311	18 42 57.37	38 11.34 N	23 18.56 E	1.79	0.08	0.40	1.00	A	9	2
	810311	21 22 3.43	38 13.61 N	23 16.58 E	3.94	0.06	0.30	0.70	B	9	2
	810311	22 18 37.87	38 7.89 N	23 18.79 E	8.07	0.08	0.40	0.70	A	11	1
	810312	1 0 54.16	38 1.13 N	23 0.24 E	0.90	0.12	0.50	7.20	C	10	0
	810312	3 49 39.27	38 13.52 N	23 16.56 E	4.85	0.04	0.20	0.60	B	9	0
	810312	5 12 46.83	38 13.48 N	23 16.97 E	5.64	0.08	0.40	0.60	B	8	3
	810312	6 33 22.66	38 3.50 N	22 55.12 E	0.23	0.10	0.40	3.80	C	7	0
	810312	7 3 35.85	38 3.45 N	22 55.82 E	5.78	0.01	0.20	0.20	B	6	0
	810312	10 8 15.89	38 13.40 N	23 14.31 E	6.54	0.09	0.50	0.70	B	8	2
5*	810312	15 58 1.57	38 8.19 N	23 6.49 E	8.07	0.08	0.40	0.90	B	10	2
*	810312	17 33 14.83	38 3.36 N	22 54.39 E	5.83	0.07	0.30	0.70	B	9	2
6*	810312	17 51 44.42	38 5.54 N	23 2.68 E	8.52	0.07	0.30	0.70	B	10	2
	810312	20 24 28.19	38 8.28 N	23 6.77 E	7.69	0.10	0.50	1.10	B	10	1
*	810312	21 21 11.56	38 2.53 N	23 13.33 E	9.21	0.06	0.30	0.40	B	10	3
*	208312	22 20 18.67	38 2.32 N	23 12.98 E	3.89	0.10	0.30	0.60	B	10	5
	810312	22 23 46.60	38 2.44 N	23 18.04 E	3.84	0.07	0.50	1.00	B	9	0
	810313	0 24 24.36	38 0.97 N	22 59.88 E	1.02	0.10	0.60	7.50	C	8	0
*	810313	0 31 47.99	38 14.12 N	23 15.46 E	9.11	0.07	0.40	0.40	B	10	3
	810313	2 17 20.32	38 5.35 N	22 56.95 E	9.40	0.06	0.40	0.60	B	9	1
	810313	3 21 18.43	38 14.39 N	23 15.30 E	6.78	0.03	0.20	0.30	B	7	2
	810313	10 3 52.62	38 13.63 N	23 16.19 E	6.53	0.07	0.50	0.90	B	10	0
	810313	12 45 41.38	38 13.72 N	23 16.45 E	3.08	0.08	0.40	1.10	B	8	3
*	810313	12 50 45.63	38 13.98 N	23 15.58 E	7.97	0.08	0.30	0.50	B	9	5
*	810313	14 35 36.23	38 5.81 N	23 10.61 E	5.55	0.08	0.40	0.60	A	9	2
	810313	15 31 52.19	38 12.42 N	23 16.24 E	2.28	0.08	0.40	1.30	B	9	2
	810313	16 33 25.94	38 14.49 N	23 15.65 E	7.21	0.09	0.50	0.80	B	10	1
	810313	19 7 13.06	38 3.58 N	23 2.60 E	7.03	0.11	0.30	0.60	B	11	5
	810314	1 14 54.43	38 13.48 N	23 14.95 E	7.94	0.08	0.50	1.10	B	10	0
•	810314	2 0 15.54	38 8.00 N	23 6.74 E	9.00	0.07	0.40	0.50	B	10	2
•	810314	2 33 26.56	38 13.71 N	23 15.19 E	9.06	0.11	0.50	0.60	B	11	2
7*	810314	5 49 12.03	38 13.41 N	23 14.91 E	9.59	0.09	0.40	0.50	B	11	4
9*	810314	11 52 36.10	38 13.67 N	23 14.96 E	8.36	0.12	0.50	0.90	B	10	3
8*	810314	12 57 6.82	38 11.04 N	23 14.85 E	11.02	0.12	0.30	0.90	A	9	6
*	810314	19 23 16.00	38 13.50 N	23 14.82 E	10.06	0.11	0.40	1.00	A	10	4
•	810314	20 20 22.70	38 6.76 N	23 9.98 E	13.23	0.09	0.40	0.50	A	11	5
•	810314	21 24 18.09	38 13.33 N	23 15.68 E	9.84	0.12	0.50	0.80	A	11	4
•	810314	22 22 13.33	38 8.95 N	23 7.68 E	7.37	0.11	0.40	0.80	A	11	3
*	810314	23 55 58.57	38 13.54 N	23 15.42 E	9.25	0.11	0.40	0.60	A	10	4
10*	810315	0 40 31.96	38 13.88 N	23 14.96 E	9.25	0.11	0.40	0.70	A	12	4
11*	810315	7 0 52.21	38 14.18 N	23 15.74 E	10.01	0.10	0.40	0.70	B	12	2
*	810315	10 55 47.39	38 13.82 N	23 14.67 E	10.72	0.10	0.50	0.60	A	11	2

Table 2 – *continued*

	Date	Origin Time	Latitude	Longitude	Depth	RMS	ERH (km)	ERZ (km)	Q	No. of Readings P	S
12*	810315	10 56 55.81	38 7.78 N	23 5.85 E	10.36	0.08	0.40	0.60	B	11	3
	810315	12 47 44.99	38 11.95 N	23 12.37 E	4.77	0.10	0.40	0.70	B	12	2
13*	810315	14 19 9.89	38 9.65 N	23 11.28 E	7.85	0.07	0.30	0.40	A	11	3
*	810315	15 47 59.73	38 14.02 N	23 16.38 E	8.33	0.11	0.50	0.70	B	12	3
•	810315	17 34 59.12	38 7.02 N	23 11.91 E	4.57	0.10	0.40	0.70	A	12	2
•	810315	15 9 29.04	38 7.04 N	23 6.57 E	10.91	0.12	0.50	0.70	B	11	3
14*	810315	18 50 21.89	38 10.27 N	23 9.92 E	8.06	0.07	0.30	0.40	B	10	4
•	810315	19 59 26.72	38 9.20 N	23 7.42 E	9.08	0.09	0.40	0.40	B	11	3
15*	810315	20 51 14.72	38 9.08 N	23 17.36 E	9.67	0.06	0.20	0.40	A	10	4
	810316	0 11 4.01	38 8.58 N	23 9.45 E	3.79	0.08	0.30	0.90	B	12	2
	810316	3 26 17.68	38 13.17 N	23 14.95 E	10.68	0.10	0.60	1.10	A	12	0
	810316	3 52 12.80	38 5.25 N	23 10.42 E	2.70	0.09	0.40	1.10	A	12	0
	810316	5 11 10.33	38 7.28 N	23 12.51 E	2.86	0.10	0.40	0.80	A	12	2
*	810316	5 23 42.93	38 13.20 N	23 15.02 E	9.93	0.13	0.50	0.60	A	12	5
16*	810316	10 32 41.86	38 13.86 N	23 15.27 E	11.78	0.10	0.50	0.60	A	11	3
17*	810316	10 37 42.47	38 13.52 N	23 15.01 E	12.24	0.07	0.40	0.50	A	11	2
18*	810316	16 31 52.74	38 8.66 N	23 7.41 E	9.76	0.10	0.40	0.70	B	12	5
19*	810316	17 37 45.07	38 8.38 N	23 10.90 E	7.09	0.07	0.30	0.70	A	11	3
	810316	18 28 14.75	38 7.65 N	23 6.23	10.24	0.06	0.50	1.20	B	8	0
20*	810317	0 32 29.12	38 8.36 N	23 7.49 E	10.20	0.12	0.50	0.70	A	11	3
*	810317	2 1 8.47	38 14.29 N	23 16.42 E	9.88	0.11	0.40	0.70	B	11	4
21*	810317	2 2 11.89	38 9.86 N	23 8.08 E	8.95	0.09	0.40	1.00	B	11	3
22*	810317	2 12 52.75	38 14.04 N	23 16.11 E	12.25	0.09	0.40	0.90	B	11	2
•	810317	3 12 30.62	38 14.71 N	23 15.27 E	12.02	0.09	0.50	1.00	A	11	3
*	810317	4 5 6.42	38 7.79 N	23 7.66 E	7.68	0.13	0.60	0.90	A	11	4
*	810317	4 49 34.45	38 14.39 N	23 15.91 E	11.99	0.12	0.50	0.80	B	11	3
*	810317	10 50 19.20	38 14.24 N	23 15.40 E	12.08	0.07	0.40	0.50	A	10	3
*	810317	14 4 3.66	38 9.25 N	23 8.45 E	9.76	0.08	0.40	0.60	A	11	2
23*	810317	14 6 3.32	38 9.50 N	23 13.54 E	9.61	0.09	0.30	0.60	A	12	4
	810317	16 51 10.27	38 12.19 N	23 12.96 E	3.45	0.10	0.30	0.90	B	12	3
24*	810317	20 39 22.53	38 13.37 N	23 15.12 E	8.88	0.09	0.30	0.80	A	12	4
25*	810317	22 24 3.79	38 14.15 N	23 14.19 E	13.40	0.10	0.50	0.60	A	12	3
26*	810317	23 8 19.16	38 9.77 N	23 13.55 E	8.34	0.06	0.20	0.50	A	12	4
	810317	23 52 49.86	38 15.62 N	23 14.82 E	3.93	0.07	0.30	1.60	B	10	3
*	810318	0 53 27.75	38 4.05 N	22 52.78 E	5.85	0.15	0.60	0.90	B	11	3
*	810318	3 55 39.76	38 13.82 N	23 14.89 E	10.25	0.11	0.40	0.50	A	11	5
*	810318	6 43 58.30	38 13.67 N	23 14.76 E	9.74	0.12	0.70	0.90	B	10	2
*	810318	6 53 23.85	38 13.20 N	23 15.12 E	11.01	0.11	0.70	1.00	A	9	1
•	810318	7 36 55.36	38 14.43 N	23 16.63 E	8.86	0.08	0.30	0.60	B	12	3
*	810318	10 29 27.92	38 11.68 N	23 4.67 E	8.04	0.12	0.50	1.10	B	11	3
	810318	14 19 39.81	38 6.86 N	22 41.23 E	18.24	0.09	0.90	1.50	C	11	1
	810318	15 38 1.12	38 6.65 N	22 40.87 E	16.17	0.09	0.70	1.20	C	9	3
	810318	18 55 30.40	38 10.87 N	23 7.11 E	3.56	0.11	0.60	1.30	B	10	0

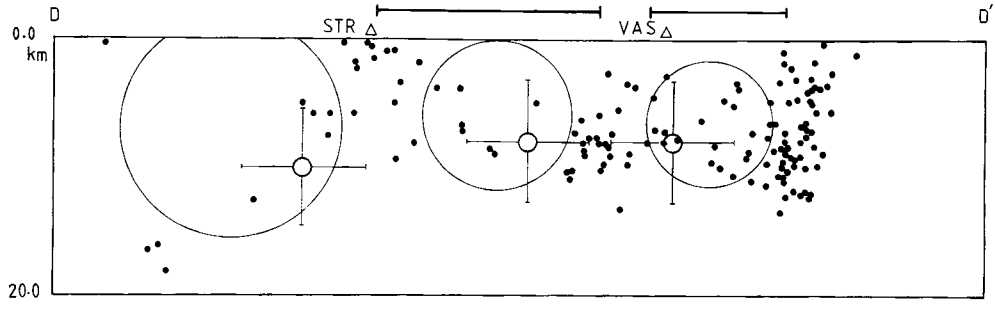

Figure 2. The section DD' from Fig. 1 with all events projected on to it. The location error of the main events are indicated by error bars. The radius r of the circles is calculated from $M = r^3 \times 1.5 \times 10^{-3}$ (m)^3 where M is the geometric moment determined from long-period body waves [1]. Bars indicate the extent of surface faulting.

v_p/v_s ratio (of 1.83) and varying P-wave velocity. Travel-time curves were plotted and rms residuals examined in the manner described in earlier work (Berberian 1982; Soufleris *et al.* 1982; Deschamps & King 1984). These indicated that a P-wave velocity of 5.7 km s^{-1} was a slightly better half-space model. This was adopted and the 70 events were relocated using v_p/v_s values from 1.60 to 2.0. The variation of rms residuals were least for the original model with a ratio of v_p/v_s of 1.83.

The bias of residuals as a function of distance suggested the possibility that a two layered model might be preferable to a half-space; various models were tested. The best, with a 2 km thick 4.5 km s^{-1} surface layer overlying a 5.9 km s^{-1} half-space produced locations with

marginally improved residuals. We do not know whether this improvement really signifies improved locations, but, more importantly, the locations were little different from those obtained with the single layer models.

As a final test of depth resolution, a few events of different depths in each subregion were chosen and located at fixed depth for a half-space with various *P*-wave velocities and v_p/v_s ratio. The resulting rms arrival time residuals were then plotted against depth. Most events had their minimum rms within the depth error estimated by HYP071 and none were more than 50 per cent outside.

In addition to the 70 events carefully tested, a further 63 are employed in the later discussion of a total of 133 events (Table 2). Those included did not change epicentre by more than 3 km when located in the three principal models outlined above; the half-space models with *P*-wave velocities of 6.0 and 5.7 km s^{-1} and the two layer model. The depth locations of some of these events is poor and this should be noted in the interpretation of Fig. 2. The hypocentral parameters, presented in Table 2 are for the model with v_p = 5.7 km s^{-1} and $v_p/v_s = 1.83$.

3 Aftershock locations

The locations and depths of all of the 133 aftershocks are shown in Figs 1 and 2. On the basis of the foregoing tests we consider that most of the events are located to within ± 2 km in epicentre and ± 4 km in depth. A few events at the western end may be less well located (see Table 2). These are retained since they represent real activity at the western end of the fault system despite poorer locations. The events marked with an asterisk in Table 2 are thought to be located within ± 1 km in epicentre and ± 2 km depth. Fig. 1 is an epicentral map and Fig. 2 a longitudinal cross-section. Some of the events are shown on cross-sections in Fig. 3. All the events lie predominantly between the normal faulting on the north and south sides of the Gulf with very few in the footwall of the north-dipping faults. This contrasts with the locations for the 1978 Thessaloniki earthquakes (Soufleris *et al.* 1982) where many events lay in the footwall of the main fault. The length of the aftershock zone is about 60 km and the width about 20 km. The events form three clusters, one on the Perakora peninsular, one west of Porto Germano and one near Platea (see Fig. 6 for place names). The shallowest reliable location is 3.6 km and few events are deeper than 10 km. Some of the events at the west end of the zone give depths greater than 15 km. Only one of these events (14.19 GMT on 18.03.81 of Table 2 and 'a' of Fig. 1) may be regarded as a reliable location and remained deeper than 15 km for all of the tests. However, it is at the edge, and slightly outside the array so its location may be in error if significant lateral variations of velocity structure occur.

In support of the possibility that the greater depths of some of the west events is real, it is worth noting that the first main event (in the same region) was also slightly deeper than the other events. Furthermore, as we shall see later, it involved a significantly greater rupture area which could have extended deeper than elsewhere (Fig. 2).

The aftershock activity is apparently greater in the east than in the west. Some of this is due to the better station coverage in the east allowing well located events to be selectively found there. However, the effect is certainly real. In other earthquakes it has been noted that aftershock activity is least at the end of the fault where rupture initiates and greatest at the end where if finishes (Eaton, O'Neill & Murdock 1970; Berberian 1982; Yielding *et al.* 1981). The same effect appears to be true for the Corinth sequence taken as a whole.

In the longitudinal cross-section in Fig. 2 the positions of the main events are shown. Approximate location errors are indicated by vertical and horizontal bars although the depth location, which was independently constrained by waveform modelling [1] is rather better

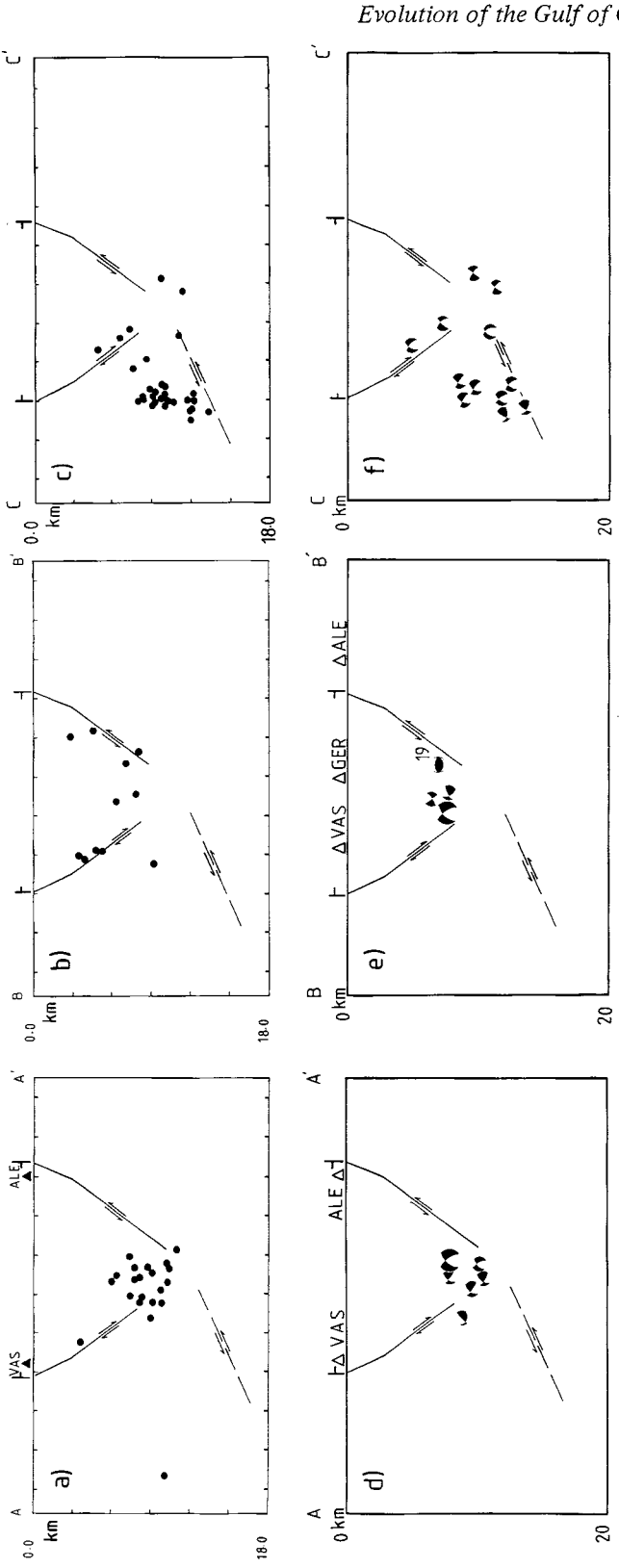

Figure 3. The cross-sections marked in Fig. 1. The positions of the faults are shown (see text for discussion) and the location of the main events (2: February 25) for section (d) and (3: March 4) for section (e) are indicated by enlarged fault plane solutions. Only well located aftershocks are included in the section (a–c) and are indicated by solid dots. Locations accuracy is about twice the dot size. Sections (d–f) show the fault plane solutions projected in the vertical plane for some of the events in (a–c). (The hemisphere represented is the one behind the plane of the paper.)

than shown. The main events lie between the clusters of aftershock activity noted in the epicentral distribution. This suggests that de-stressed regions associated with the main event faulting are relatively free from aftershocks compared to regions where the motion on the main fault planes increased stress. To determine whether this view is reasonable circles with radii determined by the moment of each event are added to the figure. The circles are mainly an aid to the eye and are not intended to suggest that the rupture areas are circular. The circles are positioned to enclose their corresponding main event and as few aftershocks as possible. In none of the cases does this put the event origin near the centre of its corresponding rupture area. In the case of the first event this is significant. It apparently ruptures to the west stopping in a region near to where a magnitude 5.3 earthquake caused damage on shore in 1954 (Vita-Finzi & King 1984, adapted from Papazachos *et al.* 1982). The rupture direction of the second event is not clearly defined because of uncertainties in the location of event 2 [see 1]. The third event apparently ruptured to the east but a bilateral rupture is possible because of errors of location. The simplest rupture system based on the foregoing is that the first two events nucleated in or near the complex faulting of the Perakora peninsular (Vita-Finzi & King 1984) with the first-rupturing west and the second east. The third event then ruptured further east along an antithetic fault. The delay between the first and second events was then presumably associated with the motion of many faults in the Perakora region and the delay between the second and third by the transmission of stress between the main fault and the antithetic fault (possibly associated with the motion of many faults at the intersection of faults I, J and K (indicated in Figs 4 and 10). Other possible event rupture sequences do not permit such a simple cause and effect description that allows one event to trigger another by stress transfer in the brittle zone and requires some other method of stress transmission such as a creep instability below the brittle zone on fault K.)

The number of aftershocks located here is not yet sufficient to allow the relation between events 1 and 2 to be discussed further. However, there are enough good locations to examine the relation between the second and third events more closely. Cross-sections for the events in the east are drawn in Fig. 3(a, b, c) for the best located events (i.e. from among the 70 events marked with asterisks in Table 2). Only events within 2 km of the projection lines

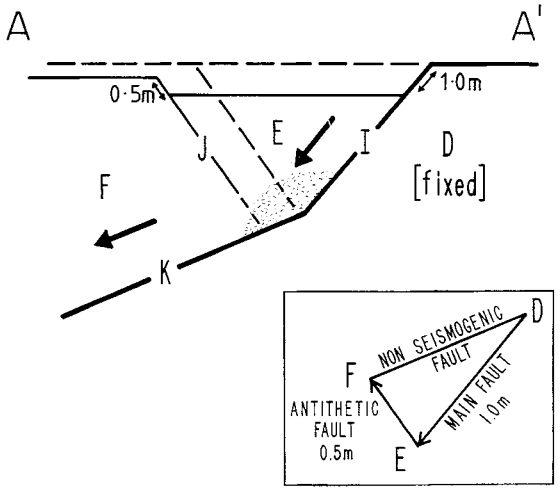

Figure 4. A block model of the faulting near to section AA' of Fig. 1. The hatched area corresponds to the aftershock region in Fig. 3(a). Dip angles come from the main event fault plane solutions as described in the text and amplitudes are from the surface breaks.

shown in Fig. 1 are used. This limit is adopted because the surface faulting is incoherent for distances greater than this. Marked on each section are lines indicating the likely positions of the main faults. From the surface to a depth of 3 km the dip is based on the angle of the surface faulting and below this depth the dip is taken from the main event fault plane solutions [1]; (the northward dip of the southern fault from event 2 and the southward dip of the northern fault from event 3). In Fig. 3(d) the location of the second main event is added to those of the aftershocks and in Fig. 3(e) the third main event is added. Both are indicated by a larger diameter fault plane solution. Although neither lie exactly on their supposed causative faults they are much nearer than their location errors require.

The morphology of the Gulf of Corinth with emergent southern and sinking northern coasts requires that the main southern fault continues to the north below its projected intersection with the antithetic fault (see [1]). This fault is shown as a dotted line in the figures. An estimate of the dip of this non-seismogenic fault can be made on the basis of a block model. We first note that in Fig. 3(a) the aftershocks are restricted to the lower part of the wedge of the block between the faults thus suggesting that, in cross-section, the deformation in the region of AA′ in Fig. 1 may be approximated in the manner shown in Fig. 4. The faults I and J in the figure have dips corresponding to the fault plane solutions of the second and third of the main events. Where the section AA′ crosses the main fault and the antithetic fault both had surface breaks with approximate average displacements of respectively 1 and 0.5 m. This information about the fault angles and displacements allows a vector triangle to be drawn (inset in Fig. 4) which determines the relative motions of the blocks labelled D, E and F. The orientation and displacement of fault K separating blocks D and F is consequently specified. Since three active faults cannot meet some internal deformation of the blocks must occur. The aftershocks along section AA′ are restricted to the base of block E (shaded in Fig. 4) and we suggest that most of the internal deformation is restricted to this region.

4 Aftershock fault plane solutions

Reliable fault plane solutions using upward-going rays were obtained for events in the eastern part of the aftershock sequence. Lower focal sphere projections with polarity readings are shown in Fig. 5. These are replotted in Fig. 6. The vertical cross-section solutions in Fig. 3(d, e, f) are from the same set. The focal mechanisms for the main events used in the figures are taken from [1].

The event indicated by R (in Fig. 6) was the largest event that occurred after the three main events and was recorded both locally and on distant stations. It was used as the reference for positioning the relocated events in [1]. Using both the local data and the teleseismic data a well constrained fault plane solution can be obtained and is shown in Fig. 7.

Normal faulting is indicated by all the fault plane solutions although some have varying amounts of left and right lateral strike-slip in addition to the extensional component. A distinction between fault planes and auxiliary planes cannot be made, but, with two exceptions, an auxiliary plane can be chosen such that the consequent slip vector is similar to that of the main events. The two different events (6 and 19 in Fig. 6) have north–south striking auxiliary planes and represent east–west extension.

The fault plane solutions of the events are also shown in Fig. 3(d, e, f). The solution for the second main event is shown in Fig. 3(d) and the third event is added to Fig. 3(e). In all cases, the projection is for a hemisphere behind the plane of the paper. The sections again indicate the overall similarity of the aftershock solutions to the main shocks although there

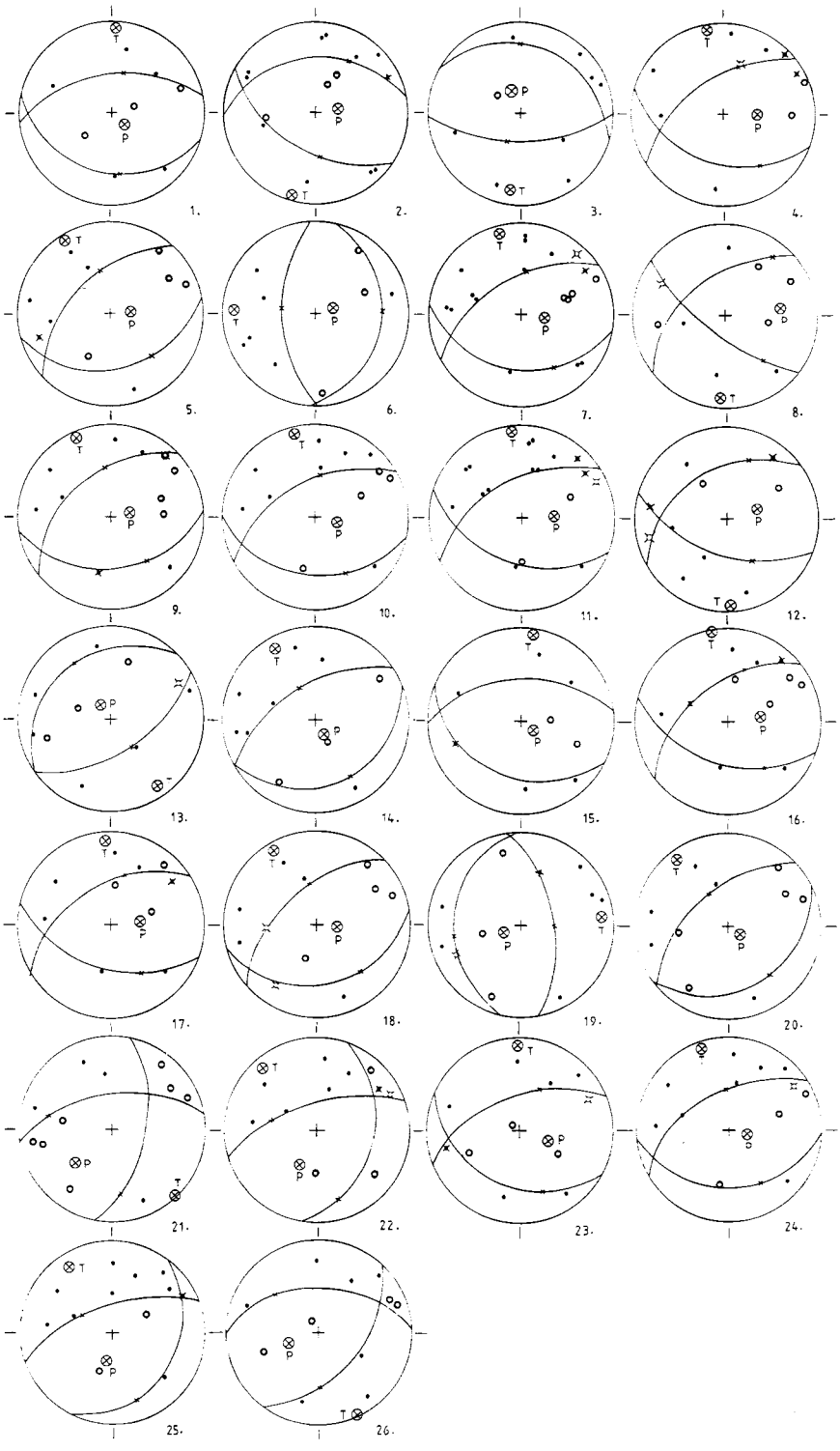

Figure 5. Fault plane solutions for the events numbered in Table 1. Upward-going rays are employed but the projections are for the lower focal hemispheres.

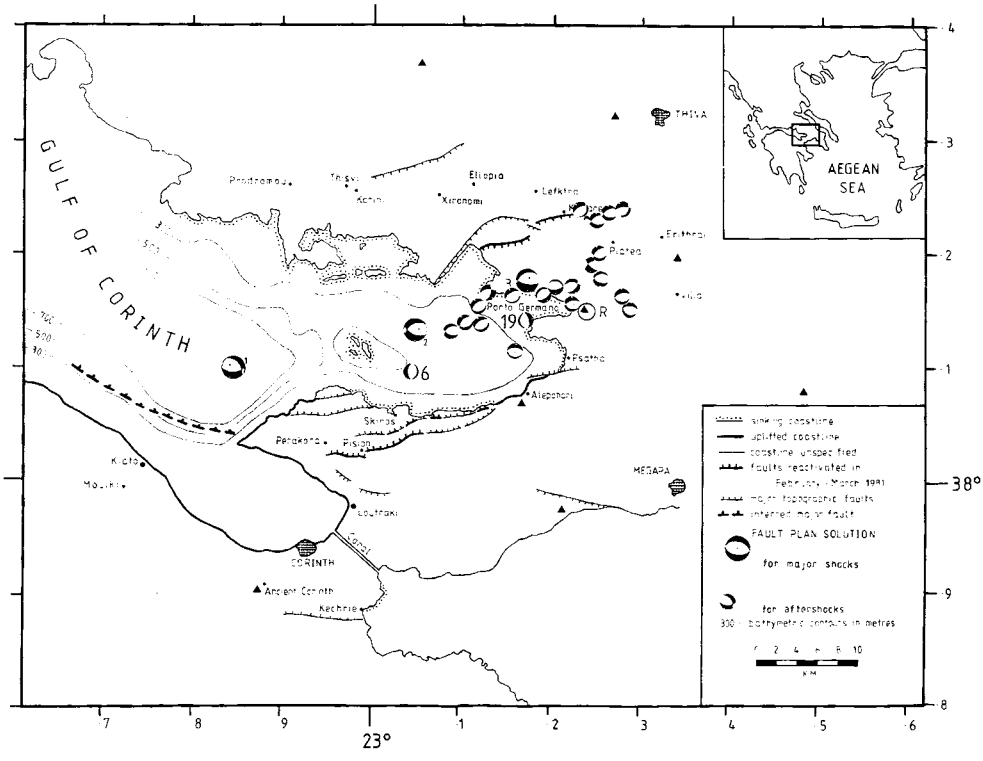

Figure 6. Fault plane solutions for the major events from [1] and for some of the aftershocks. The lower focal hemisphere is shown for all events. The numbers identify the events with transverse extension referred to in the text.

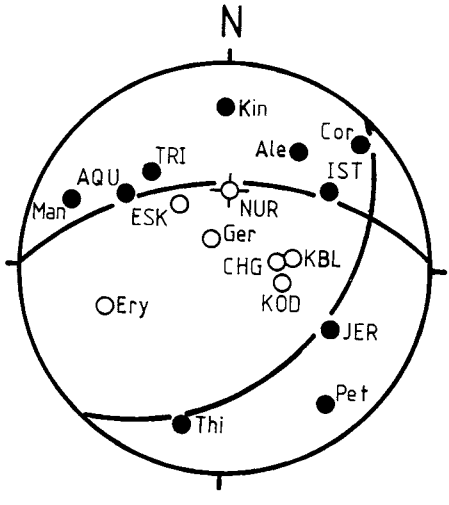

Figure 7. Fault plane solution for the largest aftershock m_b 5.5 which occurred on March 7 at 11.34 GMT. The readings in the solution are for vertical component stations. Local stations are indicated with lower case letters in the identification code and WWSSN long-period readings with fully capitalized codes. For the long-period data the crustal velocity was taken to be 6.8 km s^{-1} and for the local data the layered model used in this paper was adopted. In both cases a depth of 10 km was used. The planes strike at 42° and 90° and dip at 46° and 52° respectively.

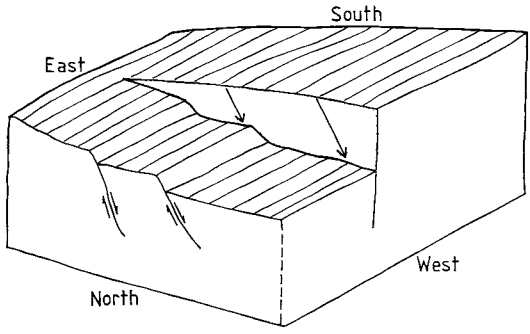

Figure 8. A schematic diagram of the end of the main southern faulting near to Psatha (see Plate 1). The fault strikes N90°E and dips at 80°N. The hade of the slickensides is 60°W.

is a scatter. Only one of the anomalous events is plotted on these sections because of the projection distance. The anomalous events are of interest. A possible explanation for faulting perpendicular to the main trend is discussed in [1] in relation to surface features. Perpendicular tensional structures are associated with ground warping between offset fault segments in the region south of Lefktra. One of the anomalous fault plane solutions (19) is down dip of this feature. However, the mechanism described in [1] explains surface features and does not obviously extend to features at greater depth. Although understanding these features will have to await more information, it is apparent that geologically young normal faults perpendicular to the main trends and with substantial throws about 100–200 m (perhaps 10 per cent of the three of the main faults) are common features. They apparently relate to changes of throw and style of the main faulting. This can be observed most clearly, in the field, near to Psatha where the main southern fault loses displacement from 250 m to zero over a distance of little more than 1 km. Plate 1 shows the feature photographed from the west and nearly along strike and Fig. 8 shows a diagrammatic interpretation of the structure from a less oblique perspective. Before the main fault disappears it is very steeply dipping and the motion (from slickensides that can be seen beside the road and along the shore) takes on a substantial left-lateral component. A number of similar, but less well defined, features appear between Perakora and Psatha, on the Perakora peninsular and near to Porto Germano.

5 The evolution of the Gulf of Corinth

Morphologically the Gulf of Corinth is apparently extending to the east. It is a major feature north of the Perachora peninsular and is absent 30 km to the east around Villia. The main southern faulting near to Skinos which has a throw of more than 1 km and extends along the southern side of the Gulf disappears to the east of Psatha. Most of the antithetic faulting in the northern Gulf is submerged although it appears on land west of Platea and then extends to almost due north of the same village. This is shown schematically in Fig. 10(a). The surprising feature is that the most eastward manifestation of the extending Gulf is apparently the antithetic faulting near Platea.

Clearly it is possible that the end of the Gulf of Corinth is behaving anomalously, perhaps because of pre-existing lines of weakness, and that under 'normal' conditions, antithetic faulting follows rather than precedes the surface appearance of the main fault. However, the morphological observation seems clear and the following discussion suggests that what we observe in the eastern gulf may well be common. As we shall explain it is both mechanically reasonable and explains in a simple fashion an otherwise perplexing aftershock distribution.

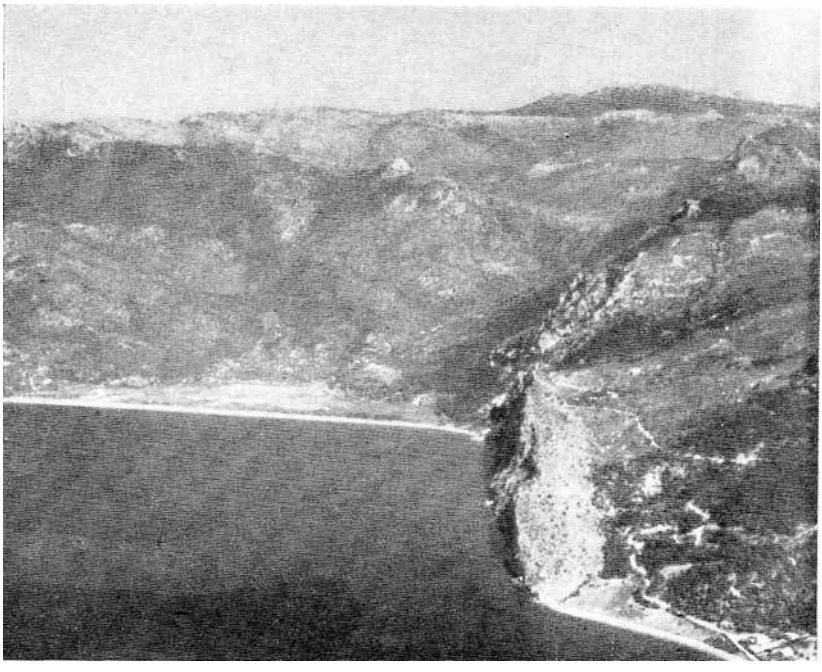

Plate 1. Oblique aerial view looking east towards the termination of the main faulting near to Psatha. The fault is nearly vertical with a throw of 250 m in the foreground. The old erosion surface in the background is not cut by an extension of the same fault. Fig. 8 is a diagrammatic interpretation of the structure.

[*facing page* 688]

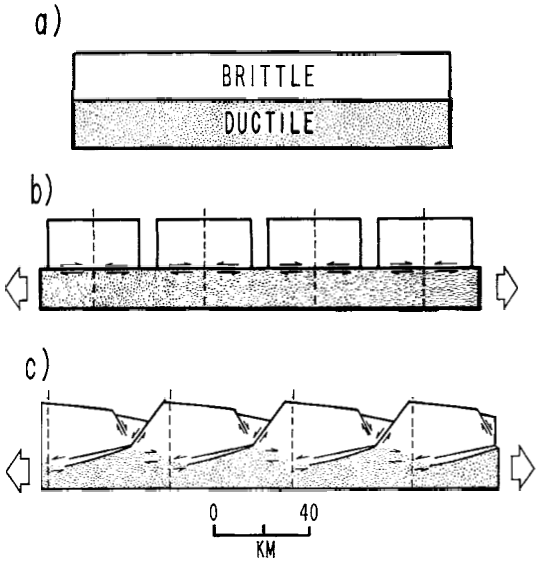

Figure 9. A descriptive model of the development of listric normal faulting. (a) shows a brittle body overlying a ductile material. When the system is stretched a structure like (b) will form in the absence of gravity. Shear deformation develops near the boundary between the two bodies. Dotted lines indicate positions where no relative displacement occurs between the brittle material and the underlying ductile material. The Earth is under gravity which prevents the formation of tensile fissures except near the surface. Near surface shear failure is constrained to a high angle by the surface boundary conditions (Anderson 1951). It is apparent from reflection data (see the references in the text) that the surface faults connect in some way with the ductile shear zone. The data do not appear to resolve whether the faults are curved or incorporate one or more angular bends as indicated in this paper.

In Section 3 and Fig. 4 it was suggested that the surface deformation and aftershocks of section AA′ of Fig. 1 could be explained by the presence of a non-seismogenic fault at depth with a shallower dip. The shallowing of the dip of normal faults with depth is recognized on many reflection profiles. In the broadest terms the mechanical reason can be seen from Fig. 9. The upper crust extends in a brittle way whereas the lower crust deforms in a more uniform fashion. This leads to finite shear strain between these layers. Since the brittle surface also fails in shear but at a steep angle, a connecting process is to be expected. It appears to operate in the way we indicate (e.g. Wernicke & Burchfiel 1982; Burchfiel 1983; Frost & Martin 1982) although at shallower depths than we suggest for the Corinth region.

Fault surfaces do not form simultaneously but by a process of spreading from initiation regions. Where these latter are positioned may be expected to control the form and evolution of fault systems. A particular question is whether a fault starts at the surface and extends down or starts at depth and extends up. It is difficult to predict this behaviour from our knowledge of material properties. Note that we are talking about the long term evolution rather than individual rupture events (e.g. Das & Scholz 1983).

Fig. 10(b, c, d, e) shows the evolution of the fault system assuming upward movement. Each section corresponds to a stage of evolution in time and the parts of the Gulf that have reached the corresponding stages are indicated on a schematic map (Fig. 10a). The first section (Fig. 10b) shows the non-seismogenic fault (K) starting to enter the brittle layer. Unable to extend by creep processes a stress system is set up that may be approximated by an edge dislocation. The next fault section that forms is the antithetic fault J initiating from the surface (Fig. 10c). Geometric constraints prevent the faults J and K from meeting

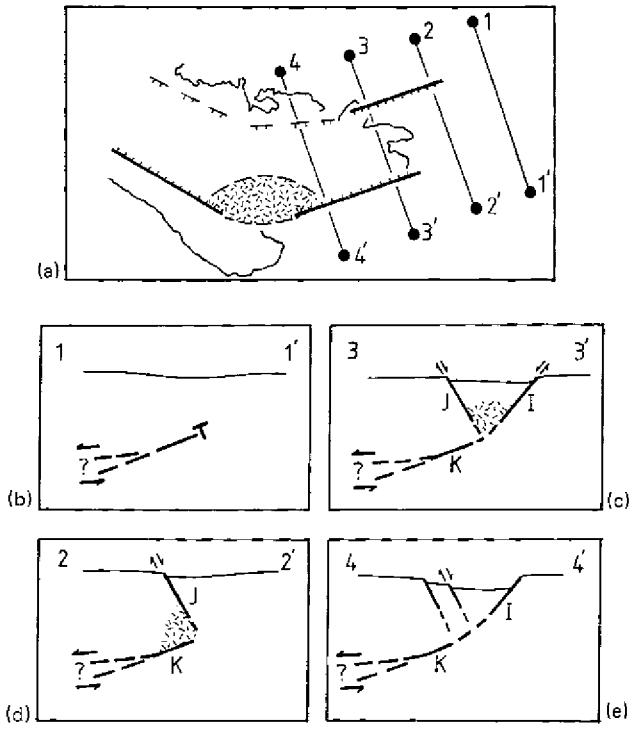

Figure 10. A schematic map of the faulting in the Eastern Gulf of Corinth. The sections b–e correspond to those marked on (a) and to the time evolution of the system discussed in the text.

and require compensating deformation. This is indicated by hatching and the deformation corresponds to the aftershock zone of Fig. 3(c) (corresponding to CC′ in Fig. 1).

Although fault J can accommodate some deformation, it cannot accommodate a large displacement of K. A new fault I forms; constrained in angle by the conditions described in Fig. 4. It is this fault that reaches the surface from below (Fig. 10d) to become the main fault. In regions where both this fault, and fault J move the aftershock deformation lies mainly between faults I and J; a situation corresponding to Fig. 3(a) (AA′ on Fig. 1). Further fault evolution will then develop the connection between K and I and may develop further antithetic structures by a repetition of the process of Fig. 9 or develop a curved fault plane or both. We do not have the data to constrain this phase of evolution.

It is pertinent to ask why an antithetic fault can appear before the main fault appears and why this faulting should start from the surface and extends downwards. An answer to the second question can be suggested by noting two features of surface rocks. First they are weaker and more readily fractured than deeper rocks. Secondly and perhaps more significantly, they are prefractured and more inhomogeneous than deeper rocks and thus provide 'defects' which are both larger and more abundant from which faulting can initiate. In engineering materials surface defects are one of the most common sites of failure initiation. The same should certainly be true in the Earth.

An answer to the first question is provided by Fig. 11 which shows the horizontal tensile strain above a buried edge dislocation calculated using results quoted by Head (1954). The dotted line in Fig. 11 represents the strains for a dislocation corresponding to the end of a horizontal fault plane and the solid line to a plane dipping at 15° to the left of the figure.

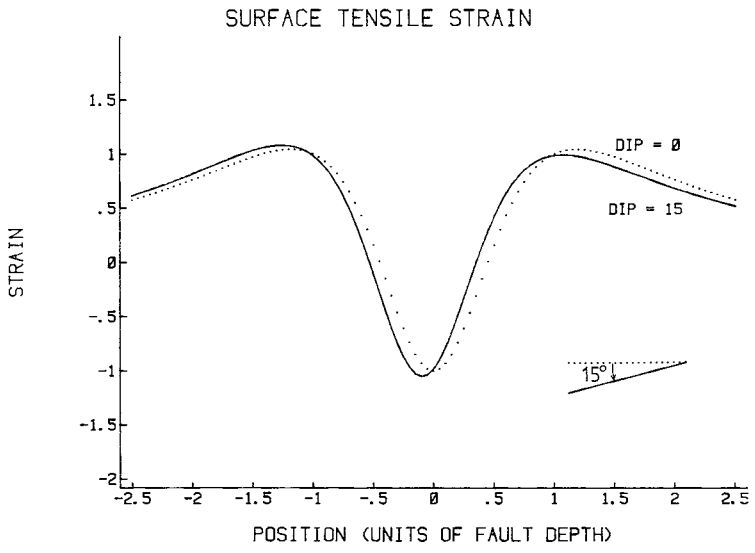

Figure 11. Surface tensile strain above a buried edge dislocation calculated using the results of Head (1954). The dotted line represents strains for a dislocation corresponding to the end of a horizontal fault plane and the solid line to a plane dipping at 15° to the left of the figure.

The strain pattern for the former is symmetrical and the extension of tensile fissures is equally favoured in the position of the final main fault and in the position of the antithetic fault. For the plane dipping at 15°, the antithetic location is favoured. The strain is increased by 5 per cent in the antithetic location and reduced by 8 per cent in the main fault location. The effect is not great but sufficient to suggest that the evolution suggested in Fig. 10 is mechanically plausible.

6 Discussion

The foregoing discussion provides a simple description of an evolving rift which makes sense of the aftershock results and broad morphological features. Two features may be noted which suggest complexity not incorporated in the model. The first concerns the observations in [1] that if the south-dipping nodal plane of the third event is identified with the surface ruptures then a poor agreement results between the surface observation of horizontal slip (average 15°E) and that determined seismically at depth (25°W). One possibility is that the surface ruptures have no simple relation to fault motion at depth but this seems unlikely in view of the extent of the surface faulting. A second possibility is that the ruptures do indeed connect with the seismic faulting at depth but that the surface slip vectors are rotated by topographic stresses. Such effects have been noted elsewhere (e.g. Yielding *et al.* 1981).

A second point concerns the possibility that the graben between Alepohori and Megara which runs at an angle of nearly 90° to the Eastern Gulf of Corinth is active. We found no evidence to demonstrate that it was mechanically connected with processes in the recent earthquakes either from morphological or seismic information. Nonetheless, this structure may be important in the longer term evolution of the eastern Gulf of Corinth.

Neither of these observations is sufficiently clear to demand a more complex model than we proposed. However, they may suggest cross-structures on a substantial scale which could play a part in the kinematic evolution of the region. Vita-Finzi & King (1984) reach a similar tentative conclusion based on an examination of the morphology of the Perachora region and the region around Corinth city.

7 Conclusions

The Corinth earthquake sequence and its aftershocks are associated with the active extension of the Gulf of Corinth that is also apparent from the morphology. A surprising, but apparently clear, observation is that antithetic faulting pre-dates the creation of the main fault. This can be explained by a simple model which postulates a shallow-angle non-seismic fault at depth. The evolutionary sequence required by this model accounts for the aftershock distribution at the eastern end of the Gulf and its relation to the main shocks.

This paper emphasizes two concepts of fault behaviour that deserve consideration irrespective of the correctness of our interpretations of the Gulf of Corinth. First that aftershocks do not necessarily lie on the main fault planes and second that the manner in which rupture extends in the evolution of a fault system can have a profound influence on the geometry that results. This applies not just to the dynamic rupture associated with an individual earthquake but also to the quasi-static rupture associated with fault systems creeping or the summed effect of many earthquakes. The geological implications of this view are discussed at greater length by Vita-Finzi & King (1984). It is of interest to note that the geometry of faulting proposed here is similar to that proposed by King & Stein (1983) to explain morphological observations in the epicentral region of the 1983 May Coalinga, California earthquake. In the case of Coalinga, however, the faults move in a sense that results in overall crustal shortening and not extension as observed in the Gulf of Corinth.

Acknowledgments

The authors would like to thank Professor Papazachos who made this work possible, and also the Mayor of Corinth and General Zervas of the Greek Army who both provided important assistance for the field-work. Geoffrey King would like to thank Keiiti Aki and others of his group for useful discussions and to Keiiti Aki for financial support at MIT where this work was written up. The project was funded by the Royal Society, the Natural Environment Research Council No. GR3/3904, INAG and NSF grant CEE 82-06456. This is Cambridge University Department of Earth Sciences' contribution No. 532 and IPG contribution No. 815.

References

Anderson, E. M., 1951. *The Dynamics of Faulting*, Oliver & Boyd, Edinburgh.

Berberian, M., 1982. Aftershock tectonics of the 1978 Tabas-e-Golshan (Iran) earthquake sequence: a documented active 'thin- and thick-skinned tectonic' case, *Geophys. J. R. astr. Soc.*, **68**, 499–530.

Burchfiel, B. C., 1983. The continental crust, *Sci. Am.*, **249**, 3, 130–142.

Das, S. & Scholz, C. H., 1983. Why large earthquakes do not nucleate at shallow depths, *Nature*, **305**, 621–623.

Deschamps, A. & King, G. C. P., 1984. Aftershocks of the Campania-Luciana (Italy) earthquake of 23 November 1980, *Bull. seism. Soc. Am.*, in press.

Eaton, J. P., O'Neill, M. E. & Murdock, J. N., 1970. Aftershocks of the 1966 Parkfield–Chalome, California earthquake: a detailed study, *Bull. seism. Soc. Am.*, **57**, 1245–1257.

Frost, G. F. & Martin, D. L., (eds), 1982. *Anderson–Hamilton Volume: Mesozoic–Cenozoic tectonic evolution of the Colorado River region, California, Arizona and Nevada*, Cordilleran Publishers, 6203 Lake Alteras Avenue, San Diego, California 92119.

Head, A. K., 1954. Edge dislocations in Inhomogeneous Media, *Proc. Phys. Soc.*, **LXVI**, 9-B.

Jackson, J. A., Gagnepain, J., Houseman, G., King, G. C. P., Papadimitriou, P., Soufleris, C. & Virieux, J., 1982. Seismicity, normal faulting and the geomorphological development of the Gulf of Corinth (Greece): the Corinth earthquakes of February and March 1981, *Earth planet. Sci. Lett.*, **57**, 377–397.

King, G. & Stein, R., 1983. Surface folding, river terrace deformation rate and earthquake repeat time in a reverse fault environment: the Coalinga, California, earthquake of May 1983, *CDMG Caolinga Vol.*, September.

Lee, W. H. K. & Lahr, J. C., 1975. HYP071 (revised): a computer program for determining hypocenter, magnitude, and first motion pattern for local earthquakes, *Open-File Rep. US geol. Surv., 75-311,* 113.

Makris, J., 1977. *Geophysical Investigations of the Hellenides,* Hamburger Geophysikalische Einelschriften Herausgegeben von dey Geophysikalischen Instituten der Universitat Hamburg und dem Max-Planck-Institut für Meteorologie, GML, Wittenborne Shone 2 Hamburg 13.

Papazachos, B. C., Comniuakis, P. E., Hatzidimitriou, P. M., Kiriakidis, E. G., Kyratzi, A. A., Panagiotopoulos, D. G., Papadimitriou, E. E., Papaisannou, Ch. A., Pavlides, S. B. & Izanis, E. P., 1982. Atlas of isoseismal maps for earthquakes in Greece 1902–1981, *Publ. geophys. Lab., No. 4,* University of Thessaloniki.

Soufleris, C., Jackson, J. A., King, G. C. P., Spencer, C. P. & Scholz, C. H., 1982. The 1978 earthquake sequence near Thessaloniki (Northern Greece), *Geophys. J. R. astr. Soc.*, **68**, 429–458.

Vita-Finzi, C. & King, G. C. P., 1984. The seismicity, geomorphology and structural evolution of the Corinth area, *Proc. R. Soc.,* in press.

Wernicke, B. & Burchfiel, B. C., 1982. Modes of extensional tectonics, *J. struct. Geol.*, **4**, 2, 105–115.

Yielding, G., Jackson, J. A., King, G. C. P., Sinvhal, H., Vita-Finzi, C. & Wood, R. M., 1981. Relations between surface deformation, fault geometry, seismicity and rupture characteristics during the El Asnam (Algeria) earthquake of 10 October 1980, *Earth planet. Sci. Lett.*, **56**, 287–304.